Supporting Information for:

Facile, non-destructive characterization of 2d photonic crystals using uv-vis-spectroscopy

V Schöps[1,2], B Lenyk[1,2], T Huhn,[3], J Boneberg[1], E Scheer[1], A Offenhäusser[2], and D Mayer[2]

[1]Department of Physics, University of Konstanz, 78457 Konstanz, Germany
[2]Institute of Complex Systems (ICS-8), Bioelectronics, Forschungszentrum Jülich, 52428 Jülich, Germany
[3]Department of Chemistry, University of Konstanz, 78457 Konstanz, Germany

Lattice Grain Comparison

Comparing the crystallinity of the hexagonal lattices using SEM is inherently difficult, since with larger scan areas the resolution for single hole identification is lost quickly. Consequently, SEM images, which resolve the particle/hole structure do not exhibit sufficient information about a macroscopic ordering. Additionally, for very large scan areas the aperture dark spot is an inevitable artefact, leading to an inhomogeneously "illuminated" image.
However, using the strong contrast of the metal/insulator lattice created by the beads, a Moiré pattern is created, when the scanning grid line distance and particle lattice constant are of comparable size. Therefore line direction of the Moiré pattern indicates a match of the scan line distance with a crystal orientation in the hcp lattice (e.g. (1,0), (1,1), (2,0), etc.).
An example of such a Moiré Patterns are visible in figure S1. In these large scale images, a sudden change in Moiré pattern orientation can be referred to as a grain boundary and is accompanied by a dark line in the image. The interfacial assembly samples lack both sudden changes in the Moiré pattern and black lines in the image indicating a high crystallinity of these films.

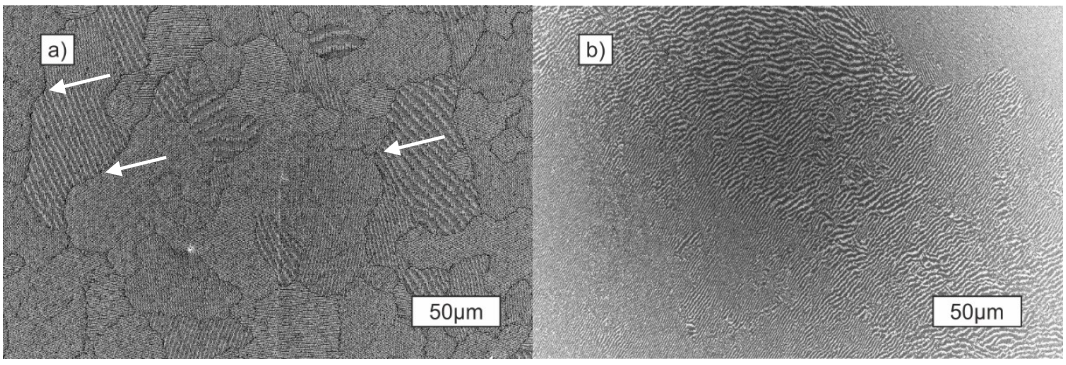

Figure S 1: Monolayers of PS beads created by a) spin-coating and b) interfacial assembly. In case of 520nm beads in a) several big, clearly separated grains with individual crystal orientation are found (arrows indicate grain boundaries), the 380nm beads in b) exhibit crystals of a rather fluent changes in crystal orientation.

The grains of the spin coating film are created during the drying of the sample and therefore underlie formation centers, around which the lattice is established and clearly separated by grain boundaries. The interfacial films are rather fluently changing grain orientation, enabling larger areas of single or similar grain orientation compared to the spin coated crystals.

Angle dependence

The samples are very sensitive regarding the angle of incidence. An increase of the peak splitting and corresponding shifts in the peak position can be observed for increasing angles of incidence, indicating a weakly dispersive nature of the photonic crystal modes.

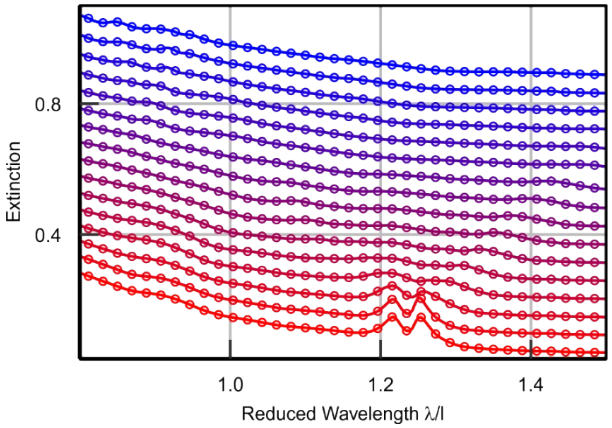

Figure S 2: Extinction spectra of a monolayer of PS beads on a polydimethylsiloxane (PDMS) substrate with increasing angle of incidence, starting at 0° for the bottom red curve in increasing in 2° steps until 30° for the top most blue curve. . The individual curves are offset for visual clarity.

Simulations

To clarify the influence of the substrate we simulated the transmission of samples with different refractive indices (figure S 3) using the FDTD software Lumerical and converting it to (1-Transmission). However, no consistent linear shift towards lower or higher energies can be obtained for increasing refractive indices. The influence of the refractive index on the peak width, shape, and position can be clearly derived. The simulated curves agree well with the experimental data.

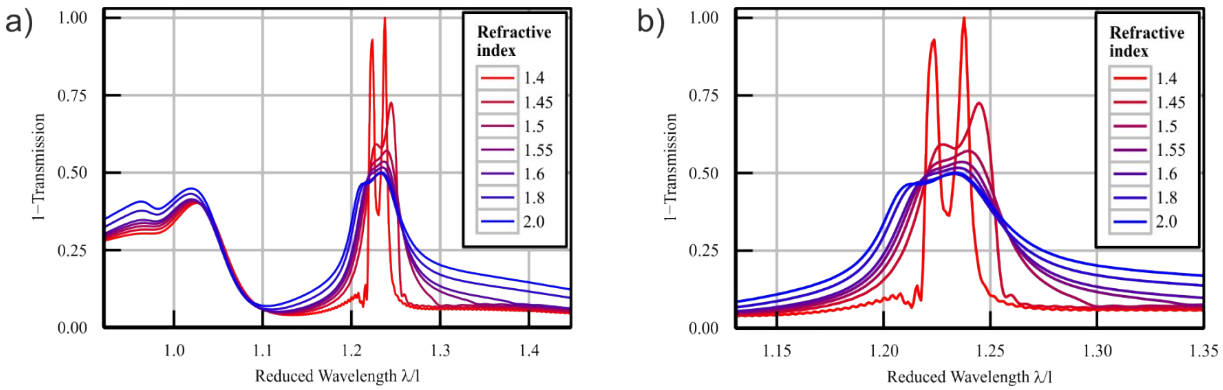

Figure S 3: Simulation of extinction spectra of a monolayer of 380 nm PS beads on substrate with different refractive indices. a) shows the entire range of reduced wavelength while b) represents the magnification of the main modes.

Coverage

The extinction spectra of PC monolayers can be utilized to correlate the crystallinity and surface coverage with the peak heights over a large range of surface coverage. Also multilayer films cause distinct features in the extinction spectra, figure S4. They will leave the lowest energy modes, used for the characterization, unaltered. However, there are new photonic crystal modes possible to occur for multilayers, which will alter the higher modes, as depicted in S4. Furthermore, the scattering background strongly increases.

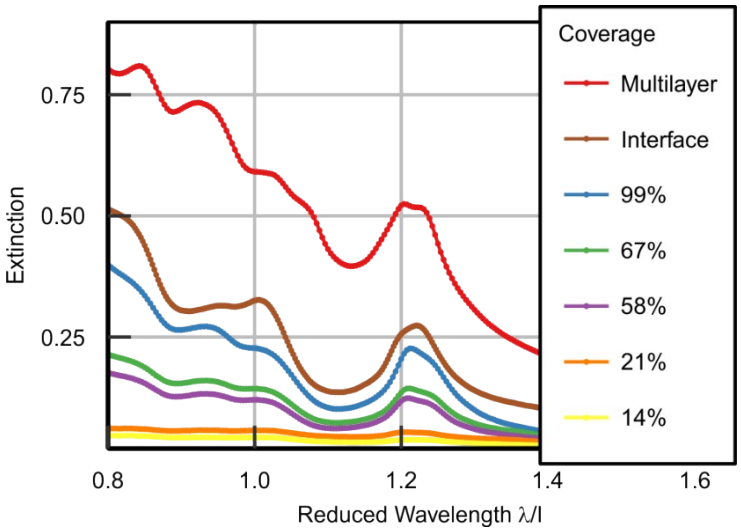

Figure S 4: Extinction spectra for monolayers of varying quality and a multilayer film. For interface assembly (brown, offset for clarity), the best resolved peaks could are found. The deposition of a multilayer results in new photonic crystal modes and an increase of the scattering background.

Spectrometer comparison

It is possible to record the radiative losses peak with both a high precision and low cost spectrometer. As depicted in figure S5, the wavelength position of the peaks are in very good agreement.

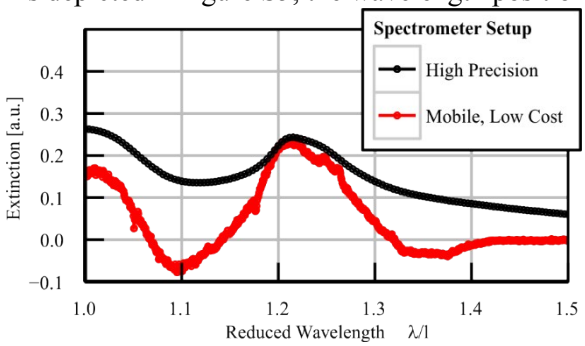

Figure S 5:Extinction plots for 520nm PS bead monolayers measured with (red) a high precision spectrometer Lambda 900 Perkin Elmer (Perkin Elmer Waltham USA) and a low cost, mobile spectrometer CCS200 (Thorlabsc Inc, Newton, USA)). The mobile spectrometer data jolted for ease of comparison. Both devices coincidently reproduce the main peak position, where the stationary spectrometer yields higher precision in the absolute value of extinction.

SEM Particle Etch

The characterization of the shadow masks created by the colloidal monolayers was done using SEM micrographs. Example picture of metal masks with different lattice constant and hole sizes are depicted in figure S6. The pictures were analyzed using the software imageJ, extracting hole sizes and lattice constants.

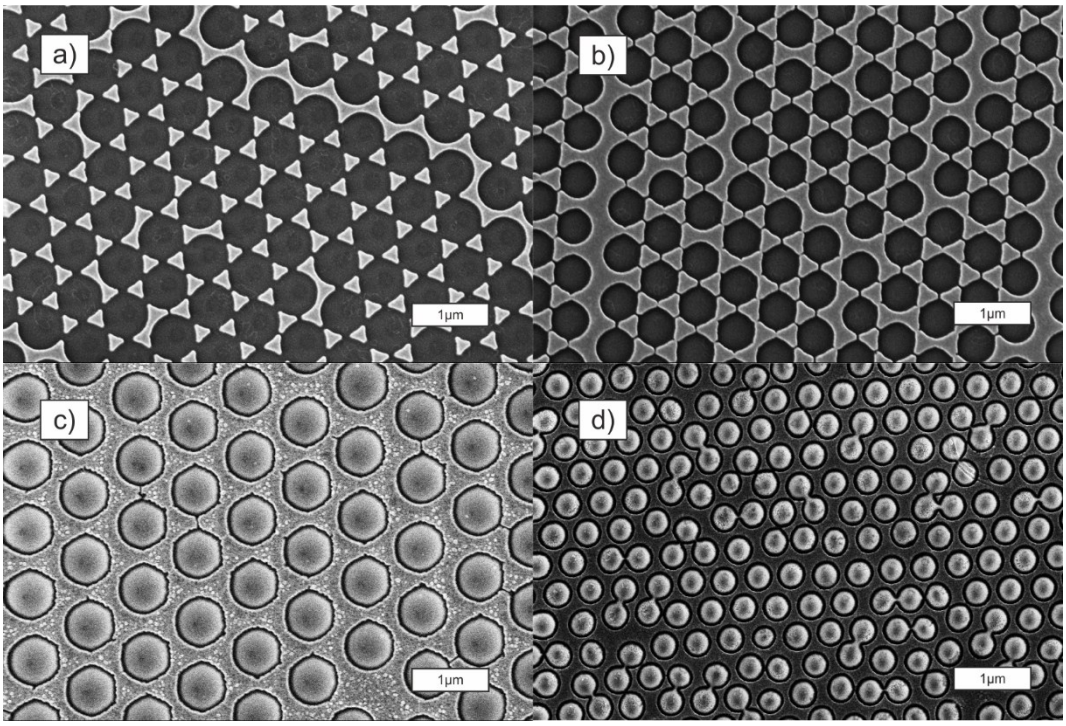

Figure S 6: Exemplary SEM images of bead imprints after metal deposition and bead removal. a) and b) 520nm bead imprints after deposition and after 4min etching in furnace, respectively. c) 720nm bead imprint, after 5min of RIE etching. d) 380nm bead imprints after 90s of RIE etching. ImageJ was used for thresholding the Images if possible and extracting the position and size of the particles.

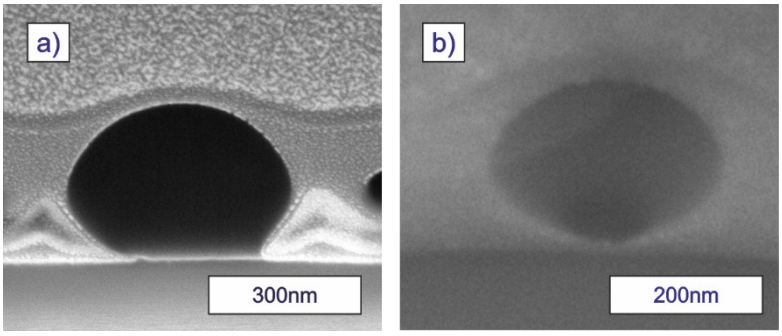

Figure S 7: SEM images of focused ion beam cross sections (Helios NanoLab 600i, FEI) of PS beads etched in a plasma furnace (a) and by reactive ion etching (RIE, b).

Different methods of etching (plasma furnace and RIE etching) have been used, both with different mechanisms and chemical compositions of the plasma. The shape of the particles is slightly different for these etching methods, see S7. However, no effect of the particle shape or surface chemistry could be observed, presumably because the layer properties are governed by the effective refractive index. As this is determined by the volumetric properties of the layer, deviations in surface chemistry or particle shape, are negligible, as long as the periodicity is maintained.

Filling Factor

Assuming a perfect isotropical etch for the individual beads, the volume filling factor f_V for a monolayer of hcp bead lattice is given by the fraction of volume occupied by PS particles V_S and by the volume of repetitive triangular unit V_T. The repetitive unit cell is generated by the volume of a equilateral triangle of length l and the height of the layer during etching, which is the particle diameter

x. The volume fraction of the spherical PS particles within this unit cell V_S is three times one sixth of the volume of a single sphere with diameter x as sketched in figure S8. This yields

$$f_V = \frac{V_S}{V_T} = \left(\frac{\pi x^3}{12}\right)\left(\frac{l^2\sqrt{3}}{4}x\right)^{-1} = \frac{\pi x^2}{3\sqrt{3}\,l^2}.$$

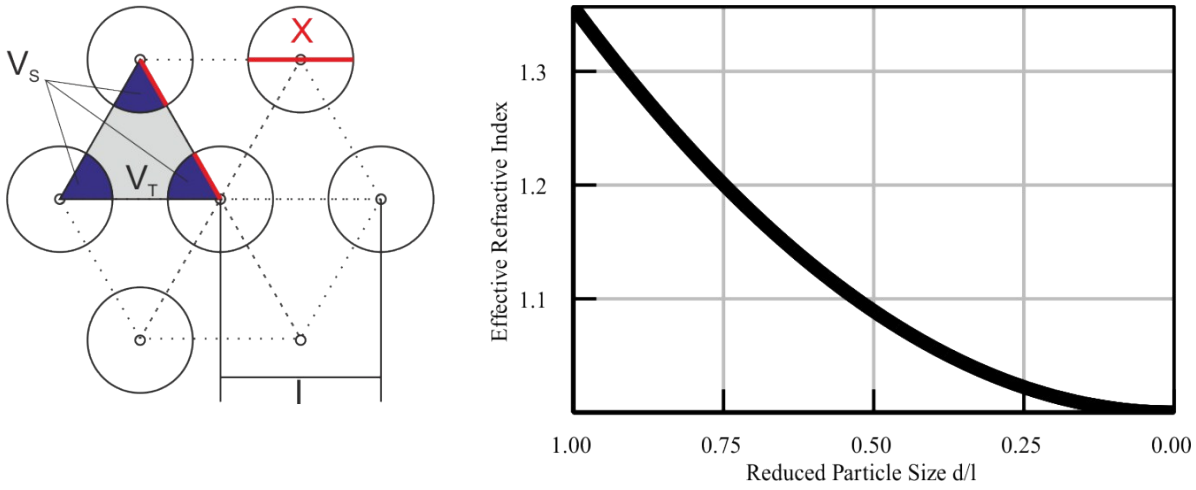

Figure S 8: a) Projected 2 dimensional geometrical model of the volume filling factor. The triangular repetition unit (grey/blue) generated by the lattice constant l is used to determine the proportional occupation of the PS spheres (blue) with diameter x. b) Calculated effective refractive index for a monolayer of beads assuming a isotropic particle etch

Thereby the lattice distance l is constant during etching, which can be assumed according to the analysis of the SEM images of the metal bead imprints in figure S6. The effective refractive index of the etched monolayer of PS beads can be calculated by

$$n_{eff} = f_V n_{PS} + (1 - f_V) n_{Air}.$$

h consequently is depending on the particle diameter by the power of two. With a refractive index of the PS spheres of $n_{PS} = 1.59$ this results in a approximately linear increase in refractive index for bigger particle diameters between 0.5 < d/l <1.

For short etching times, or big particle sizes, the holes resemble small bridges between them. This is due to local melting of the PS spheres in their contact points, seen in figure S9.

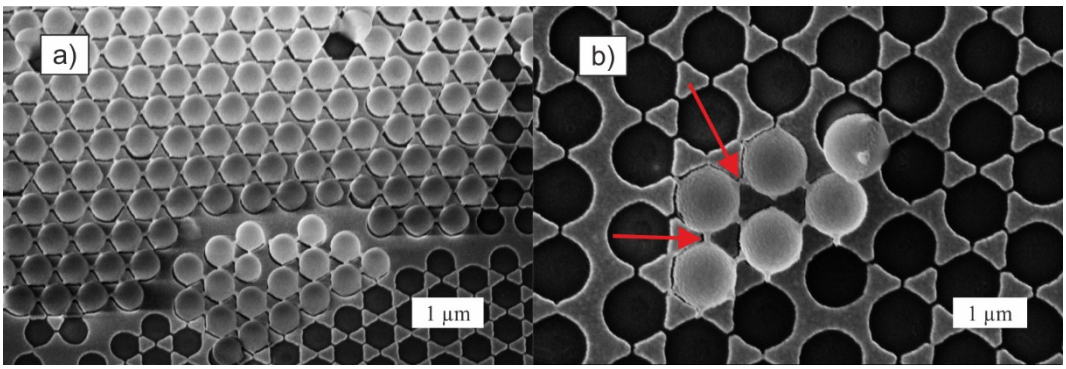

Figure S 9: Local melting of PS particles during initial plasma etching. a) 30° tilted image of a partly removed particle monolayer covered in a thin layer of Au. b) Zoom of a small patch of residual particles with red arrows pointing on the small connecting bridges in between PS particles.

Consequently, for a certain particle diameter reduction, the direct polymer connections can cause a reduced shift in refractive index compared to an ideal etch described above.